Available online at www.sciencedirect.com
SCIENCE DIRECT®
Journal of Sound and Vibration 288 (2005) 601–621
JOURNAL OF SOUND AND VIBRATION
www.elsevier.com/locate/jsvi

Some observations on uncertainty propagation through a simple nonlinear system

K. Worden[a,*], G. Manson[a], T.M. Lord[a], M.I. Friswell[b]

[a]*Department of Mechanical Engineering, University of Sheffield, Mappin Street, Sheffield S1 3JD, UK*
[b]*Department of Aerospace Engineering, University of Bristol, Queens Building, Bristol BS8 1TR, UK*

Accepted 5 July 2005
Available online 2 September 2005

Abstract

This paper discusses a number of issues relating to the analysis of uncertain systems or data in the context of (low-frequency) structural dynamics. In order to illustrate potential problems in applying 'classical' uncertainty analysis methods to nonlinear systems, a simple nonlinear system is simulated and the breakdown of two standard approaches is demonstrated on data from the system. By relaxing the requirements of the analysis, it is shown that an alternative uncertainty theory gives useful qualitative information about the system. This motivates a discussion of how uncertainty frameworks should be chosen to suit the problem in hand and leads to a clustering of uncertainty problems in structural dynamics into three types: quantification, fusion and propagation.
© 2005 Elsevier Ltd. All rights reserved.

1. Introduction

The traditional methods of engineering design are based on a cycle running from design through prototyping and validation to design update. This cycle is time-consuming and costly and is gradually yielding to a virtual process whereby prototyping and validation are carried as far as possible in computer simulation or modelling. The economic advantages of such a strategy are

*Corresponding author. Tel.: +44 114 222 7758; fax: +44 114 222 7890.
E-mail address: k.worden@sheffield.ac.uk (K. Worden).

0022-460X/$ - see front matter © 2005 Elsevier Ltd. All rights reserved.
doi:10.1016/j.jsv.2005.07.008

clear. However, there are also other considerations. For example in the arena of nuclear weapons research, current test bans place an embargo on certain types of experimental validation.

There are two obvious caveats associated with a reliance on computational simulation. Firstly, the process of validation must be as rigorous as possible and anticipate any working environment that the designed structure or system might encounter. Secondly, the modelling process should be robust to uncertainty. To elaborate on this second point, which is the subject of this paper, it is not enough to have a high-fidelity model of a system or structure without an understanding of how uncertainty propagates through the model. Consider a complex component incorporating inelastic materials, contacts, friction, etc. The model requires an initial specification of material properties, clearances and friction coefficients. The response of the model will only be as accurate as these initial values, yet the values may be subject to large uncertainty; consider the difficulty in characterising viscoelastics or even biomaterials. In a worst case analysis, the predictions of the model may prove highly sensitive to variations in the input parameters.

Another compelling reason for uncertainty quantification is the fact that the environmental and operational conditions for certain engineering projects are unknown and cannot be estimated with certainty. Alternatively, conditions can be estimated, but cannot be recreated exactly in validation experiments. Consider the design and manufacture of an in-orbit facility. In this case, aspects of the true environment, such as weightlessness and absence of drag, can be reproduced to an extent in terrestrial experiments. However, consider the design of an exploration module intended to operate on the surface of Venus. Such systems are extremely expensive and will often have only one chance to succeed. The performance of the Hubble telescope, and more recently of the Beagle explorer, are object lessons here.

Another prime motivator for uncertainty analysis is the need for risk assessment in safety critical systems. In fact, one might argue that the modern origins of the subject are here with projects like the Nuclear Reactor Safety Study [1]. One of the main regulators in the design of Structural Health Monitoring (SHM) systems for say, civil aircraft, will be the need to eliminate false assertions of damage as a result of environmental and operational variations. Such false positives and the ensuing 'no fault found' inspections would substantially increase the cost of ownership of the aircraft. Even more critical is the possibility of a false negative as a result of environmental uncertainty, with potential loss of life the result.

One traditional approach to assessing uncertainty in a response is to carry out a Monte Carlo exercise, whereby the input parameters to the model are varied over their possible values, perhaps with a given probability distribution. This allows the modeller to assemble statistical information about the response as a function of input parameter variation and ultimately specify a distribution for the model response characteristics of interest. The problem with this approach is that very many runs of the model are required for a confident estimate of the statistics, and the number of runs grows explosively with the number of input parameters considered. If the model itself is complicated, e.g. a FE model with many nodes, the cost associated with many simulations may be prohibitive.

To give an idea of the intensive nature of uncertainty calculations; in the year 2000, Los Alamos National Laboratories (LANL) in the US ran an unprecedented calculation on one of the most powerful computers in the world—the platform *Blue Mountain*. The computation essentially attempted to quantify the propagation of uncertainty through a nonlinear finite element (FE) model of a weapon component under blast loading. The specific objective of the exercise was to determine the model sensitivity to certain input parameters—preloads and friction coefficients,

etc. The calculation made use of 3968 processors from the available 6000 and used concurrently nearly 4000 ABAQUS/Explicit licences. The analysis took over 72 h and would have required 17.8 years of equivalent single-processor time [2].

An appropriate model of uncertainty is a vital element in the design and modelling procedure for high-value engineering structures and systems—this is the problem of *quantification*. As discussed later, there are numerous theoretical frameworks which allow a specification of uncertainty, the broader problem of quantification involves selecting the appropriate theoretical framework and then assigning a quantitative measure of uncertainty or risk. Given that there is more than one way of assigning a measure of risk, the problem arises of translating between them. This problem of normalisation is broadened into one of *fusion* by posing the question: given two assignments of uncertainty from different frameworks, how can one refine each estimate in the light of the extra information from the other? Equally important in the design process is a prescription for deciding how a measure of uncertainty on the inputs or specification of a problem will affect the outputs or results. This is the problem of *propagation*. Part of this problem is to find which parameters contribute most to output uncertainty. These parameters will require the most effort to estimate in the a priori specification of the problem.

The object of this paper is to illustrate the problems of quantification and propagation with respect to a particular simple nonlinear system. The reason for the choice of system is to show that even a simple nonlinear system raises questions about the applicability of standard reliability algorithms for computing uncertainty propagation. Here, it is shown that two often-used techniques break down catastrophically. It is important to raise this issue; the complex calculation at LANL described above was nonlinear. It is not intended that one should extrapolate directly from the Duffing oscillator simulated here to the complex LANL model as far too little is known about nonlinear systems with very high numbers of degrees-of-freedom. However, it is important to be aware that there are potential caveats in modelling nonlinear systems. One reason for the breakdown of the techniques applied is that the algorithms asked for probabilistic information and the problem is more suited to a different means of quantification. A possible solution for the case discussed in this paper is shown.

The layout of the paper is as follows. The next section describes the simple nonlinear system which forms the basis of the calculations here. Section 3 describes how this system leads to complex behaviour which foils attempts to build simple parametric models. Sections 4 and 5 investigate the structure of the data in more detail and suggest that it has a self-similar structure which makes a simple parametric analysis impossible. Section 6 briefly explains how and why a first-order reliability method (FORM) breaks down for the problem. Section 7 raises the possibility of using alternative uncertainty frameworks and illustrates how this is used to advantage for the nonlinear system. The paper concludes with some discussion in Section 8.

2. A simple nonlinear system

The system under investigation here is arguably the most basic nonlinear system studied in structural dynamics—the harmonically forced Duffing oscillator with equation of motion,

$$m\ddot{y} + c\dot{y} + ky + k_3 y^3 = X\cos(\omega t). \tag{1}$$

If $k_3 = 0$, the system is linear and well understood. The response is simply,

$$y(t) = Y\cos(\omega t - \phi), \tag{2}$$

where the gain Y/X and phase ϕ of the response at a given ω are unique, i.e. there is only one possible stable response. In terms of the frequency response function (FRF) of the system, the FRF is single-valued at all frequencies. If $k_3 \neq 0$, a harmonic balance approach to finding the response yields a cubic equation for the response amplitude (actually Y^2),

$$X^2 = Y^2\left\{\left[-m\omega^2 + k + \frac{3}{4}k_3 Y^2\right]^2 + c^2\omega^2\right\}. \tag{3}$$

Depending on the value of ω, this equation can have one or three real roots and thus three possible response amplitudes. The situation is illustrated in Fig. 1 which shows the system FRF. Below a certain frequency, ω_{low}, there is only a single stable solution. This is also true above a frequency ω_{high}. However, in the interval between these frequencies there are three possible response amplitudes, in decreasing order of magnitude these are $y^{(1)}$, $y^{(2)}$ and $y^{(3)}$. In practice, the solution $y^{(2)}$ is unstable and thus never observed. In summary, in the interval between ω_{low} and ω_{high} there coexists a possible low amplitude and a possible high amplitude response. Which response is actually produced in a given situation depends on the initial conditions for the system. It will be shown that this dependence is quite complicated.

The values of ω_{low} and ω_{high} can be computed by appealing to a standard result from algebra [3]. Each cubic has defined, a *discriminant* D which is a function of the coefficients. If $D<0$, the cubic has one real root, if $D>0$ it has three. As the coefficients of Eq. (3) are functions of ω, the discriminant is also. With a little help from a computer algebra package, it was shown in Ref. [3]

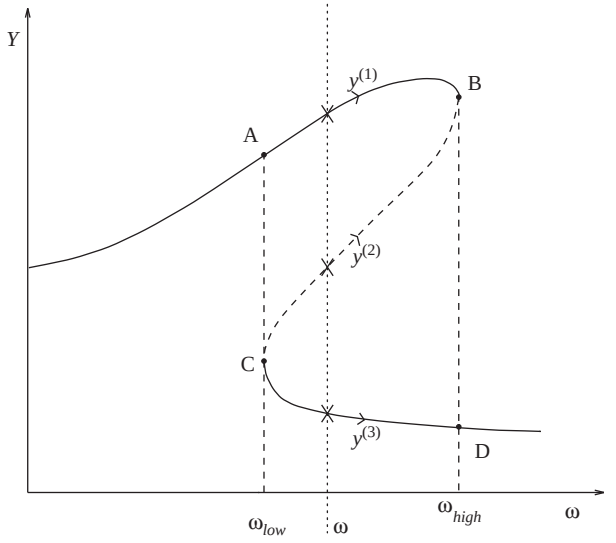

Fig. 1. Multiple solutions in Duffing oscillator FRF.

that the discriminant associated with Eq. (3) is,

$$D = \frac{256}{729k_3^6}(-64c^2k^4\omega^2 - 128c^4k^2\omega^4 + 256c^2k^3m\omega^4 - 64c^6\omega^6 + 256c^4km\omega^6 - 384c^2k^2m^2\omega^6 - 128c^4m^2\omega^8 + 256c^2km^3\omega^8 - 64c^2m^4\omega^{10} - 48k^3k_3X^2 - 432c^2kk_3X^2\omega^2 + 144k^2k_3mX^2\omega^2 + 432c^2k_3mX^2\omega^4 - 144kk_3m^2X^2\omega^4 + 48k_3m^3X^2\omega^6 - 243k_3^2X^4). \quad (4)$$

The bifurcation points ω_{low} and ω_{high} must therefore correspond to roots of $D = 0$. However, this equation is a quintic in ω^2 and can thus have five independent solutions for ω. Fortunately, it turns out in practice to have only two real roots and three complex. The lowest real root is ω_{low} and the highest is ω_{high}.

3. Uncertainty propagation: response surface analysis

When faced with an extremely expensive computation, one possibility is to establish a fast-running or *surrogate* model which approximates the response of the system or structure. Such a model is trained to reproduce the results from the true model on a given training set and can be used to interpolate over the range of input parameters for the purposes of statistical modelling. Models of this type can be as simple as a *response surface* [4]. The desired response characteristic R is obtained for a set of values of the input parameters $\theta_1, \theta_2, \ldots, \theta_n$ and a regression model of the form $R = R(\theta_1, \ldots, \theta_n)$ is estimated. The particular regression model could be as simple as a multinomial or as advanced as a Support Vector Machine. This section considers the problem of establishing a type of response surface for the 'simple' nonlinear system described in the last section.

Before attempting to characterise how uncertainty propagates through the system, a series of simulations were conducted in order to illustrate the difficulties associated with fitting a response surface for certain input parameters. Those considered here are the initial displacement and velocity of the system $(y_0, \dot{y}_0)$ and the frequency of excitation ω. The response characteristic of interest will be the amplitude of the response Y. Predicting the amplitude for the nonlinear system is non-trivial, but important, as one is essentially faced with a low or potentially high response level with the attendant consequences for fatigue, etc. Note that the problem for the underlying linear system *is* trivial as the response surface $Y = Y(y_0, \dot{y}_0, \omega)$ collapses to $Y = Y(\omega)$ as a result of the decay of transients. The remaining functional variation is captured by the standard FRF. The response surface is smooth in ω and invariant over the initial conditions.

In order to produce concrete results, it is necessary to fix the coefficients of the Duffing oscillator in Eq. (1) and the excitation level X. In order to induce strong nonlinearity, the coefficients $m = 1$, $c = 20$, $k = 10^4$ and $k_3 = 5 \times 10^9$ were taken in combination with $X = 10$. Solving the discriminant equation from Eq. (4) with these values gave $\omega_{\text{low}} = 151.98\,\text{rad/s}$ and $\omega_{\text{high}} = 190.01\,\text{rad/s}$. When compared with the undamped natural frequency of 100 rad/s for the underlying linear system, these values show that the effect of the nonlinearity is dramatic.

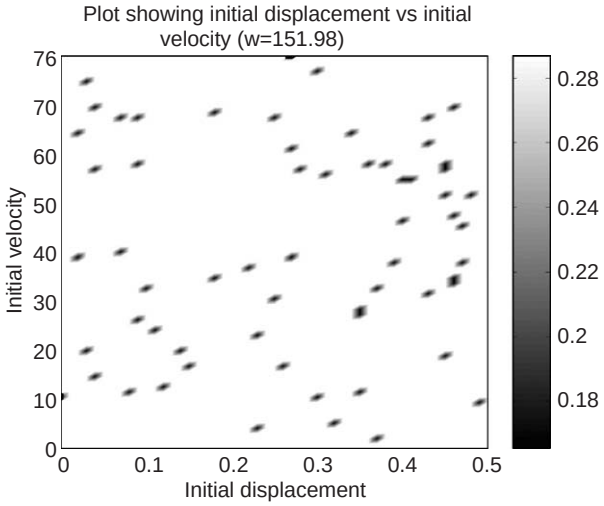

Fig. 2. Initial conditions $(y_0, \dot{y}_0)$; basins of attraction just above ω_{low}.

The first illustration shows the effect of varying the initial displacement and velocity on the response amplitude at a fixed ω just above ω_{low}. Initial displacements were taken in the range 0–0.5 and initial velocities in the range 0–76 $(0.5 \times \omega_{\text{low}})$. Each simulation, which was accomplished using fourth-order Runge–Kutta, was continued until the response had stabilised at either the low or high value. Fig. 2 shows a contour map of the response amplitude over the $(y_0, \dot{y}_0)$ plane.

Far from a smooth variation, the figure shows a dust of low-amplitude solutions against a background of high-amplitude solutions. Such a surface would be impossible to model as the low-amplitude solutions appear to be randomly distributed. Note that isolated points in the figure appear as regions as a result of the interpolative shading of the graphics package. It will be shown later that the low-amplitude points are in fact isolated.

Fig. 3 shows the amplitude map for a range of initial conditions when the driving frequency is just below ω_{high}. As in Fig. 2, the response shows dust. However, the role of the high- and low-amplitude solutions is reversed with the low amplitude providing the background. This result should not come as surprise to those familiar with nonlinear dynamics. In the literature of chaos [5], it is well known that the basins of attraction of coexistent solutions of a nonlinear dynamical system can have quite complex structure including fractal basin boundaries.

The next simulation fixed the initial displacement at zero and investigated the amplitude variation as a function of uncertainty in the initial velocity and forcing frequency. The velocity range was taken as before and the value of ω was varied between ω_{low} and ω_{high}. Fig. 4 shows the result.

A rather different aspect is shown, there appear to be vertical ridges distributed irregularly in the response. In fact, this irregularity is an artefact of the resolution. Fig. 5 shows the response over a (cross-shaped) subregion of the plot in Fig. 4 and reveals that the surface is characterised by periodically appearing ridges. One might deduce from this that there is some hope of fitting a surrogate model here as the periodicity in the initial velocity axis could be captured by, for

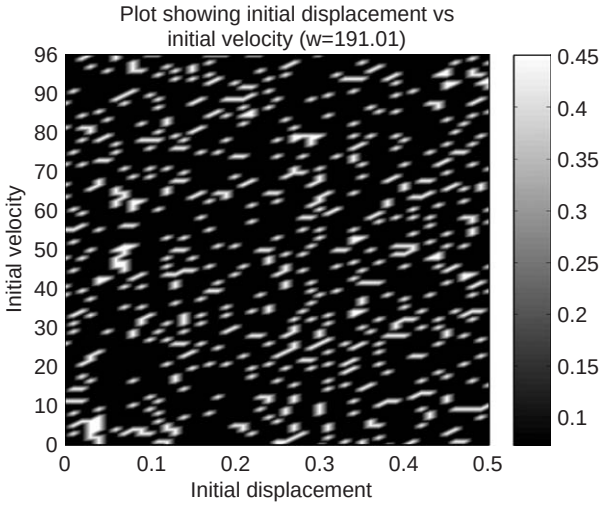

Fig. 3. Initial conditions $(y_0, \dot{y}_0)$; basins of attraction just below ω_{high}.

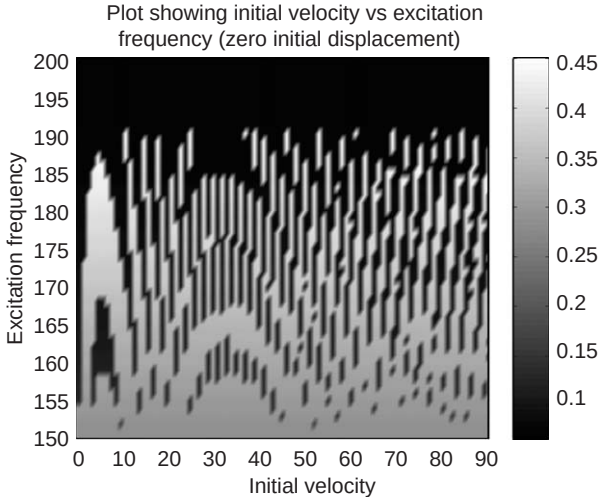

Fig. 4. Initial condition $y_0 = 0$; basins of attraction for varying $\dot{y}_0$ and ω.

example, a Fourier series. In fact this might be true in the coarse representation shown in Fig. 5, but a more close look reveals more complex structure. Fig. 6 shows a 100× magnification of a region in Fig. 5 in the vicinity of a basin boundary. There is clearly finer structure, which might on closer examination, prove to be fractal.

The final set of simulations investigated the effect of varying the initial displacement and forcing frequency. The initial velocity was fixed at zero and the initial displacement was taken in the interval (0,0.5) with ω between its high- and low-bifurcation points as before. Fig. 7 shows the response map for the coarse mesh of simulations.

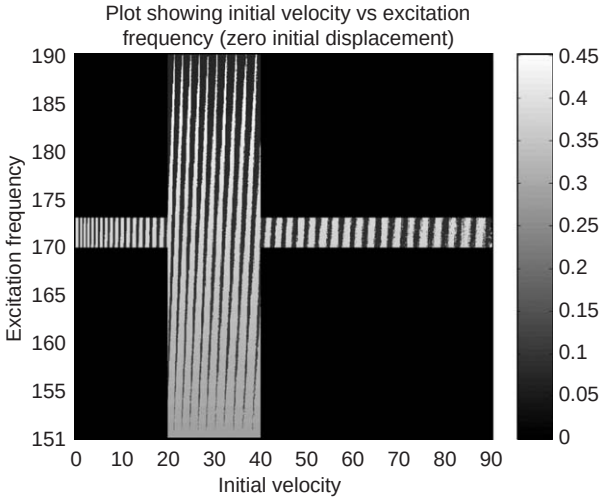

Fig. 5. Initial condition $y_0 = 0$; basins of attraction for varying $\dot{y}_0$ and ω. High-resolution subplot.

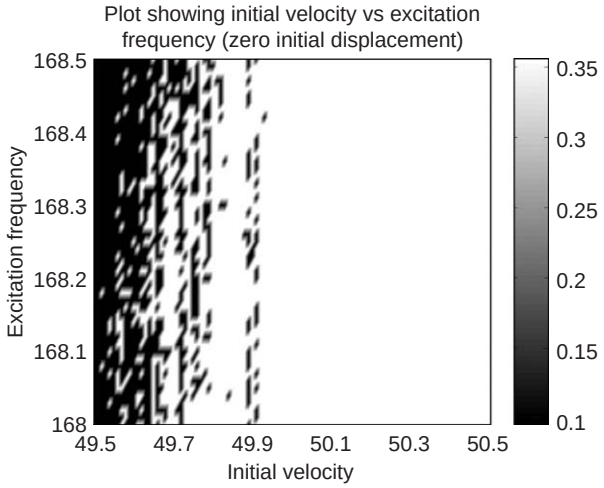

Fig. 6. Initial condition $y_0 = 0$; basins of attraction for varying $\dot{y}_0$ and ω. Vicinity of basin boundary.

Fig. 8 zooms in on the region between $\omega = 171$ and $\omega = 176\,(\mathrm{rad/s})$ with initial displacements in the range 0.22–0.28. This represents a ten-fold increase in resolution over Fig. 7. Fig. 9 shows a further 10-fold increase in resolution showing the response between ω values of 174.1 and 174.7 (rad/s) and initial displacement values between 0.255 and 0.261.

The sequence of Figs. 7–9 shows that response map has the same characteristics at three different levels of resolution. This type of scale invariance is evidence of underlying self-similarity [8]. The figures suggest that there is an underlying structure to the data; however it is far from what is required to fit a smooth response surface. The next two sections take up the question of what structure is present.

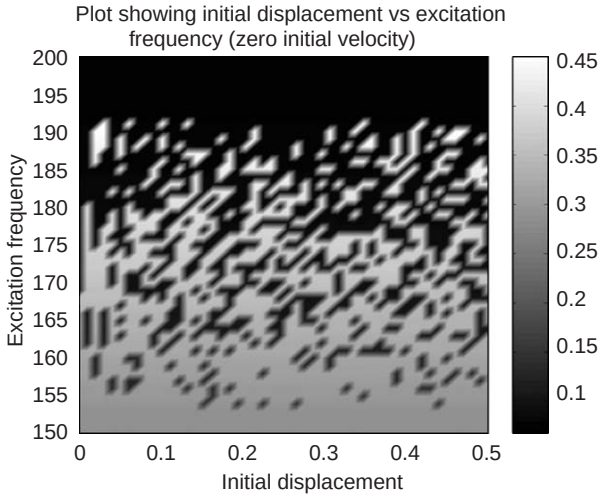

Fig. 7. Initial condition $\dot{y}_0 = 0$; basins of attraction for varying y_0 and ω.

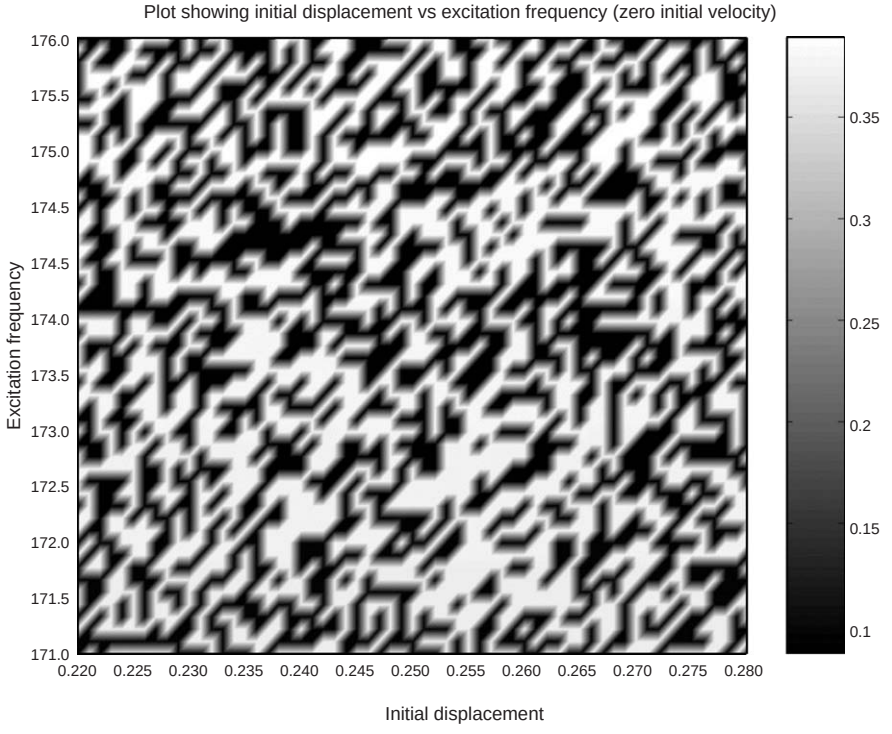

Fig. 8. Initial condition $\dot{y}_0 = 0$; basins of attraction for varying y_0 and ω. Resolution $\times 10$.

4. Fourier analysis

The first attempt to look for structure in the response data used Fourier analysis to look for periodicities in the data. In order to simplify matters by allowing one-dimensional Fourier

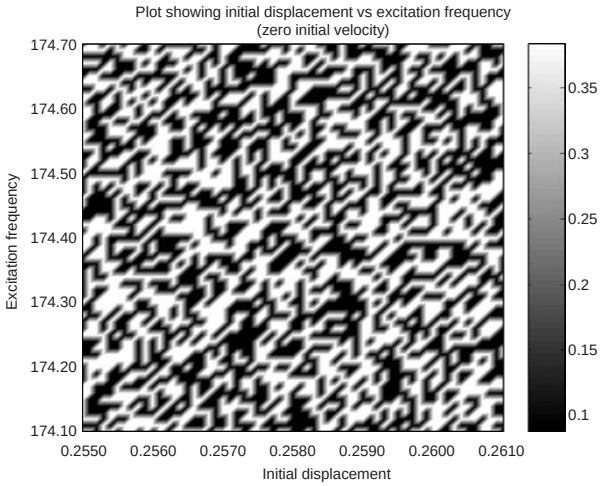

Fig. 9. Initial condition $\dot{y}_0 = 0$; basins of attraction for varying y_0 and ω. Resolution $\times 100$.

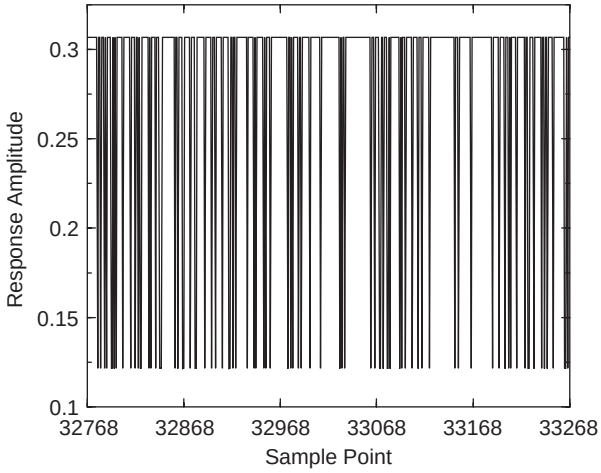

Fig. 10. Example of spatial series resulting from section of response map.

transforms, sections were taken through the (y_0, ω) response map at $\omega = 157$, $\omega = 174$ and $\omega = 187$ (all rad/s). 262,144 (2^{18}) elements were taken over the range of initial displacements at these frequencies. The analysis here will concentrate on the $\omega = 157\,\mathrm{rad/s}$ sequence. Fig. 10 shows a segment of 500 samples taken from the centre of the record.

The signal appears very similar to a pseudo-random binary sequence (PRBS), i.e. it jumps between two values at apparently random intervals. The randomness would lead one to suggest that the spectrum was broadband. Fourier transformation would be expected to reveal if this was the case or if there appeared to be significant periodicities. Fig. 11 gives the FFT of the first half of the sequence and does not appear to indicate any obvious cycles. Apart from a region of increased energy at very low frequencies, the spectrum appears flat. This behaviour is clarified considerably

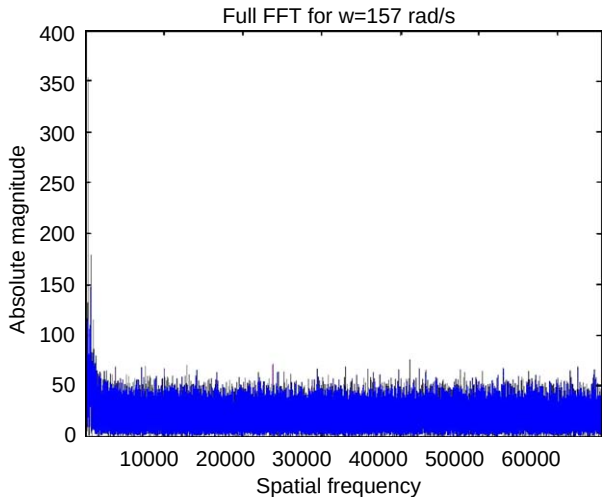

Fig. 11. Spectrum of spatial series resulting from section of response map.

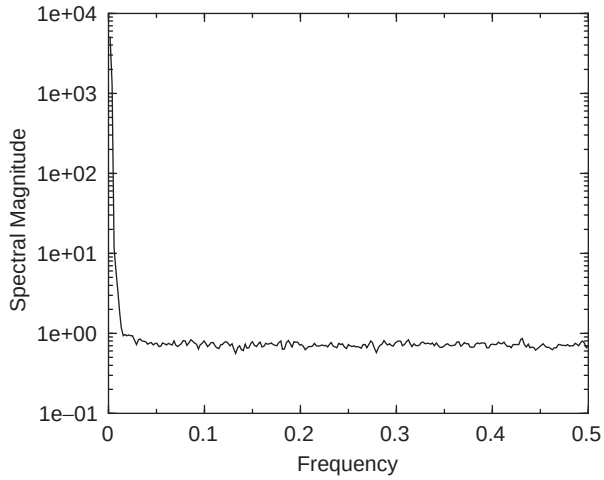

Fig. 12. Averaged spectrum of spatial series from response map.

in Fig. 12, which this time shows the power spectrum $S_{zz}(\omega)$ averaged over 256 non-overlapping segments of 512 points each. (Here, $z(x)$ denotes the spatial series. Note that strictly speaking, the abscissa of the spectrum should be wavenumber rather than frequency, this is considered here as a trivial matter of normalisation.) This implies a randomness to the sequence. However, if the sequence is truly random, the only real hope for a structural model is a probability density function. In this case, there are two discrete outcomes—high or low amplitude, so the PDF collapses to a single probability, e.g. that of low amplitude.

Summing the outcomes over the three sections gives the probability of obtaining the low-amplitude solutions as: 0.845 at $\omega = 157\,\mathrm{rad/s}$; 0.530 at $\omega = 174\,\mathrm{rad/s}$; 0.238 at $\omega = 187\,\mathrm{rad/s}$.

This sort of specification is the best that can be achieved if the spatial sequences extracted are truly random. However, randomness does not mean the complete absence of structure and the next section attempts to discover scaling or self-similar structure in the data. In many ways, this is a digression as it is not clear how the presence or otherwise of such structure would allow the refinement of a probabilistic response model. The technique used is based on the ideas of *wavelet analysis*.

5. Wavelet analysis

5.1. Wavelets

Although wavelet analysis is now widespread in engineering, for the sake of completeness and to establish notation, a brief description of the relevant wavelet theory is given. More detailed analysis can be found in Ref. [6].

Let $L^2(\Re)$ denote the space of measurable square-integrable functions $x(t)$ defined on $= (-\infty;+\infty)$ which represent analog signals with finite energy. The wavelet transform is a linear transformation on this space that decomposes a given function $x(t)$ into a superposition of elementary functions (a basis) $g_{a,b}(t)$ derived from an analysing or *mother* wavelet $g(t)$ by scaling and translation i.e.,

$$g_{a,b}(t) = g^*\left(\frac{t-b}{a}\right), \tag{5}$$

where $*$ denotes complex conjugation, b is a translation parameter indicating the locality and a is a dilation or scale parameter. The continuous Grossman–Morlet wavelet transform is defined as

$$W_g^x(a,b) = \frac{1}{\sqrt{a}}\int_{-\infty}^{+\infty} x(t)\, g^*\left(\frac{t-b}{a}\right) \mathrm{d}t. \tag{6}$$

For the function $g(t)$ to qualify as an analysing wavelet, it must satisfy appropriate admissibility conditions [6].

In much the same way as for the Fourier transform, a discrete version of the wavelet transform is available for computational purposes. Using a binary dilation and a dyadic translation, the *orthogonal* wavelet transform can be defined. A function $\psi(t)$ is called an orthogonal wavelet if the family $\psi_{m,k}(t) = 2^{m/2}\psi(2^m t - k)$ forms an orthonormal basis of $L^2(\Re)$, that is $\langle \psi_{m,k}, \psi_{n,l}\rangle = \delta_{m,n}\cdot\delta_{k,l}$, for all integer m,n,k,l, where $\langle,\rangle$ is the usual inner product and $\delta_{m,n}$ is the Kronecker symbol.

In the following, the wavelets of Daubechies [6] are used in the orthogonal wavelet decomposition,

$$x(t) = \sum_{m,k} x_k^m \psi_{m,k}(t), \tag{7}$$

where the x_k^m are the coefficients. The orthonormal basis is obtained using Mallat's pyramid algorithm [7]. Note that this algorithm is $O(n)$ and is thus faster than the FFT algorithm.

5.2. Wavelets and fractals

It is well known that stationary periodic series are invariant under translations in the time domain. As a consequence, the statistics of these processes are also invariant under translations. The Fourier series or transform are the main mathematical tools for the analysis of such translation-invariant processes.

There exist many physical signals which display invariance, not under translation but under scale change. Such signals have fractal waveforms. One important group of these waveforms is the set of statistically scale-invariant or self-similar random processes known as $1/f$ processes. Here scale-invariance means that, statistically, the process is embedded within itself at different scales. Due to the time-scale nature of the wavelet transform, it is well equipped to study such self-similar processes. In fact, it can be shown that the self-similarity of a given signal $x(t)$ implies self-similarity of its wavelet transform $W_{\psi}^{x}(a,b)$ in the time-scale domain.

The $1/f$ family of statistically self-similar random processes are formally defined as processes with a spectrum of the form [8],

$$S_x(\omega) = \frac{\sigma_x^2}{|\omega|^{\gamma}}, \tag{8}$$

where γ is termed the spectral parameter. The exponent γ is related to the self-similarity in the following sense. A random process $x(t)$ is statistically self-similar if for any real $a>0$ it obeys the scaling relation [8],

$$x(t) \equiv a^{-H} x(at), \tag{9}$$

where the equivalence means that the two processes have the same statistics. In the *strict sense*, this means all statistical moments are equal, in the *wide sense* the condition is only enforced up to second order, i.e.,

$$\overline{x(t)} = a^{-H}\overline{x(at)} \tag{10}$$

and

$$\phi_x(t,s) = \overline{x(t)x(s)} = a^{-2H}\phi_x(at,as). \tag{11}$$

In all cases, H is a constant—the self-similarity parameter. To give a concrete example of such a process, zero-mean stationary white Gaussian noise $w(t)$ has $H=-1/2$. As one might expect, the self-similarity parameter for a $1/f$ process depends only on the spectral exponent, in fact it can be shown that $\gamma = 2H+1$. Given that the spectrum of $w(t)$ is independent of frequency, it immediately follows that $H=-1/2$ and vice versa.

$1/f$ processes are of considerable interest as many physical processes exhibit the spectral behaviour given in Eq. (8).

A number of wavelet-based algorithms have been developed to study self-similar processes. The algorithm used in this paper is based on the statistical properties of the orthogonal wavelet coefficients [8].

The key result is that the variance of the orthogonal wavelet coefficients of a given $1/f$ process, takes the form,

$$\operatorname{var} x_n^m = \sigma^2 2^{-\gamma m}, \tag{12}$$

where the variance is taken over 'time' n and σ is given by

$$\sigma^2 = \frac{\sigma_x^2}{2\pi}\int_{-\infty}^{\infty}\frac{|\Psi(\omega)|^2}{|\omega|^\gamma}\,\mathrm{d}\omega, \tag{13}$$

where $\Psi(\omega)$ is the Fourier transform of the mother wavelet.

It is a trivial consequence of Eq. (12) that the log variance of x_n^m plotted against level m is a straight line with gradient $-\gamma$. It also shows that the variance of the wavelet coefficients for $1/f$ processes obey a geometric progression consistent with the statistically self-similar structure of the process. Neglecting low m effects (as described later), $1/f$ processes are characterised by the semi-logarithmic plot of the wavelet coefficient variances.

It can further be shown that wavelet coefficients are wide-sense stationary at each fixed scale m. The normalised wavelet correlation, defined as [8]

$$\rho_{n,n-l}^{m,m} = \frac{E[x_n^m x_{n-l}^m]}{\sqrt{(\mathrm{var}\, x_n^m)(\mathrm{var}\, x_{n-l}^m)}} \tag{14}$$

is a function only of the lag l for a given value of scale m.

Processes corresponding to $1<\gamma<3$, which exhibit infinite low-frequency power are known as the *fractional Brownian motions*; classical Brownian motion is a special case corresponding to $\gamma = 2$. Processes corresponding to $-1<\gamma<1$ show infinite high-frequency power and are termed the *fractional Gaussian noises*; classical white stationary Gaussian noise is a special case with $\gamma = 0$ [8].

In the case of fractional Brownian motions, the Hausdorff–Besicovitch fractal dimension D of the signal, is related to the self-similarity parameter by [8],

$$D = 2 - H \tag{15}$$

and to the spectral exponent by,

$$D = \frac{5-\gamma}{2}. \tag{16}$$

Note that the self-similarity discussed here is distinct from that usually analysed. Most often, it is the self-similarity or fractal dimension of the underlying phase space *attractor* of the nonlinear system which is the issue. Here, the concern is with the statistical self-similarity and dimension of the time-series itself.

5.3. Application to the data

In order to minimise edge effects for the spatial sequence of response amplitudes, the data from the second quarter of the range was analysed using the wavelet variance approach. This means that the record contained 65,536 points. For the first analysis, a Daubechies $D = 4$ mother wavelet was adopted. The resulting coefficient variance plot is given in Fig. 13.

The gradient of the line $-\gamma$ is zero for this signal. This might be expected from observing the flat spectrum in Fig. 12, the result is consistent with the data representing a $1/f$ process with $\gamma = 0$.

The corresponding self-similarity parameter H is $-1/2$. Note that there is some fluctuation in the plot at lower values of the level m; this is because the level m is composed of 2^m wavelet basis functions. Level 0 is simply the mean of the signal and level 1 is formed of only one wavelet, the

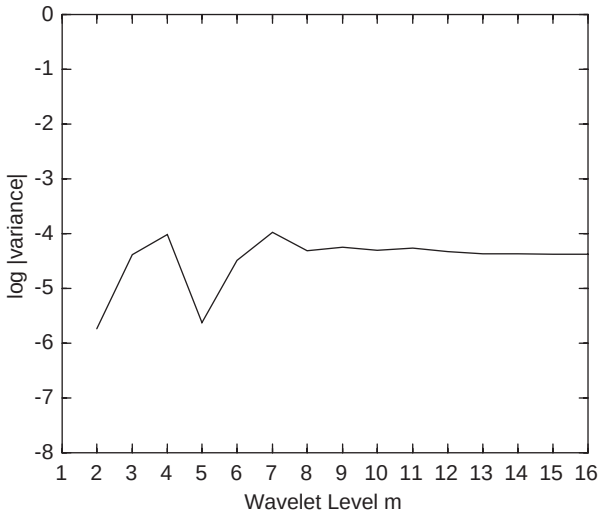

Fig. 13. Wavelet coefficient variance for spatial sequence at $\omega = 154\,\mathrm{rad/s}$.

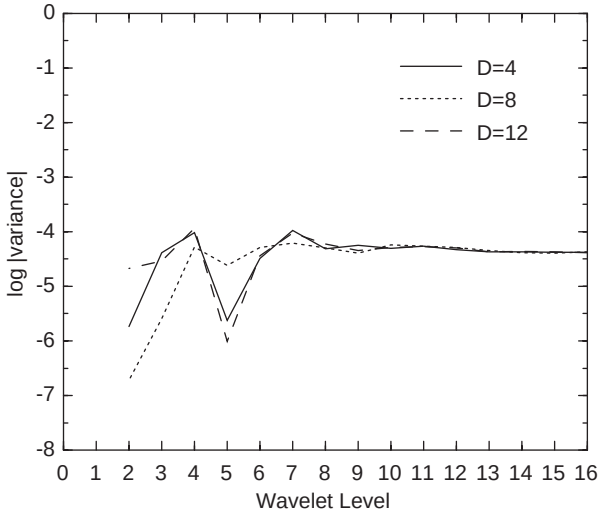

Fig. 14. Wavelet coefficient variance for spatial sequence at $\omega = 154\,\mathrm{rad/s}$. $D = 4$ (solid), 8 (dotted), 12 (dashed).

form of the particular wavelet used therefore has an effect on the lower levels and the gradient of the line should only be estimated using variances from higher levels [8].

In order to show that the result is not simply an artefact of the choice $D = 4$, Fig. 14 adds the corresponding plots for $D = 8$ and 12.

Their is evidence here to support the conclusion that the spatial sequence is statistically self-similar. The presence of some structure in the data is therefore confirmed, although it is unfortunately no help in establishing a surrogate model.

6. Uncertainty propagation: FORM

This section is concerned with the first-order reliability method (FORM). The theory and application of this approach are textbook material [9], but the salient facts will be summarised here.

As far as this paper is concerned, FORM is used to approximate the density function of a response random variable Z given the density functions of the input random variables $X_1, \ldots, X_n$. In order to estimate the cumulative density function (CDF) one must compute

$$P(Z < z_0) \tag{17}$$

for all values $z_0 \in [0, 1]$. Exchanging this problem for one involving the independent variables, one arrives at an integral,

$$P(Z < z_0) = \int \cdots \int_{z(x_1,\ldots,x_n) < z_0} p(x_1, \ldots, x_n)\, \mathrm{d}x_1, \ldots, \mathrm{d}x_n, \tag{18}$$

where $p(x_1, \ldots, x_n)$ is the joint probability function of the input variables. In geometrical terms this integral is the volume under the joint density function bounded by the *limit surface* $g(\underline{x}) = z(x_1, \ldots, x_n) - z_0 = 0$. Except in very restricted cases, this integral is analytically intractable and needs to be evaluated numerically. One approach is to use a Monte Carlo scheme, but that proves too expensive if z is expensive to compute or the probability is small. The solution is to make a change of variables. A nonlinear transformation is made which converts the vector $(x_1, \ldots, x_n)$ into a vector $(u_1, \ldots, u_n)$ where the components have independent Gaussian distributions (although it is theoretically possible to do this with the Rosenblatt transformation, it is rarely *practically* possible and the approximate Nataf transformation is used [9]). The limit surface $g(\underline{x})$ is carried into a surface $g(\underline{u})$, and the integral of interest becomes,

$$p(Z < z_0) = \int \cdots \int_{g(\underline{u}) < 0} p(u_1, \ldots, u_n)\, \mathrm{d}u_1, \ldots, \mathrm{d}u_n. \tag{19}$$

Now, although the integrand has factored into a sequence of univariate Gaussians, the domain of integration ($g(\underline{u}) < 0$) is usually very complicated and the integral is still analytically impossible. At this point, a second approximation is made and the limit surface is replaced by a hyperplane $g_l(u_1, \ldots, u_n) = a_1 u_1 + \cdots + a_n u_n + a_0 = 0$. (This is FORM, if the limit surface is approximated by a quadratic, the result is the second-order reliability method—SORM.) The hyperplane is computed by taking a first-order Taylor approximation about the point on the true limit surface nearest the origin (the mode of $p(\underline{u})$). This point is called, for obvious reasons, the Most Probable Point or MPP and the distance of this point to the origin is usually denoted β. The integral,

$$p(Z < z_0) = \int \cdots \int_{g_l(\underline{u}) < 0} p(u_1, \ldots, u_n)\, \mathrm{d}u_1, \ldots, \mathrm{d}u_n \tag{20}$$

can be carried out analytically and the result is $\Phi(-\beta)$ where Φ is the standard Gaussian CDF.

Note that the result depends critically on the availability of the gradient $\nabla_{\underline{u}} g$. (In SORM, the Hessian of g is needed.) It will be shown later that this leads to serious problems for the simple nonlinear system discussed earlier.

First consider a linear system for illustrative purposes. This is obtained by setting $k_3 = 0$ in Eq. (1). The problem considered here is simply that of obtaining the PDF of the response amplitude under the assumption that the input parameters ω (forcing frequency) and x_0 (initial condition) have independent uniform distributions on the intervals $[160, 180]\,\mathrm{rad/s}$ and $[0, 0.005]\,\mathrm{m}$. In order to have a basis for comparison later, a Monte Carlo calculation was carried out. 5000 points were taken from the (ω, x_0) distribution and the response of the system in Eq. (1) was computed using a Runge–Kutta scheme in Matlab. The 5000 responses were used to estimate the PDF using kernel density estimation (KDE) [10], and the result is as shown in Fig. 15. The overall result is undersmoothed as the calculation of the smoothing parameter attempted to preserve the steep sides of the distribution.

The next calculation computed the CDF of the response distribution by taking 100 values over the range of the amplitude and running a FORM calculation for each. The PDF was then obtained by fitting a least-squares polynomial to the CDF and differentiating the result analytically. The result is shown in Fig. 16. In this particular case, the calculation required approximately 5/6 times the number of function evaluations of the Monte Carlo method but gave a much smoother representation of the PDF. This shows the utility of the FORM method. The software used here is a minor modification of the FERUM package [11].

The next calculations restored the cubic term to Eq. (1). In the first, a Monte Carlo approach with 5000 evaluations yielded the density in Fig. 17. The result is clearly bimodal reflecting the bifurcative nature of the problem.

In the next calculations, a FORM analysis was attempted. Several runs were taken in an attempt to get values for the CDF, all failed. This is due to the fractal nature of the response surface as discussed in the last section. The FORM software has to approximate the derivatives of the limit-surface in the $\underline{u}$-space, but in this case this is a linear transformation of the limit surface in the $\underline{x}$-space which is self-similar. In practice, this means that every neighbourhood of the Most Probable Point contains high- and low-amplitude responses. In an attempt to form the derivative, the software continually reduces the step-size in order to stabilise the discrete difference, but this

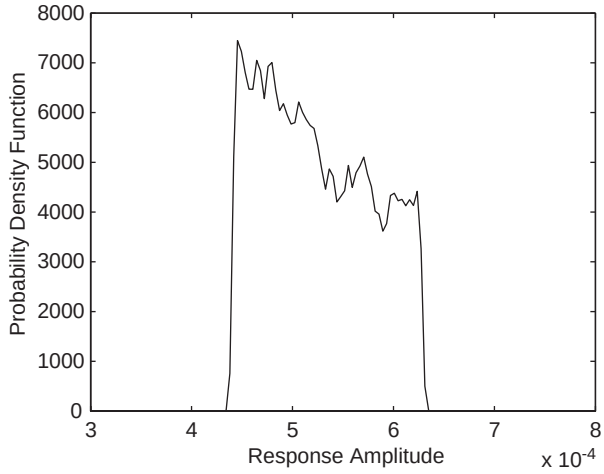

Fig. 15. Kernel density estimate of linear system response PDF.

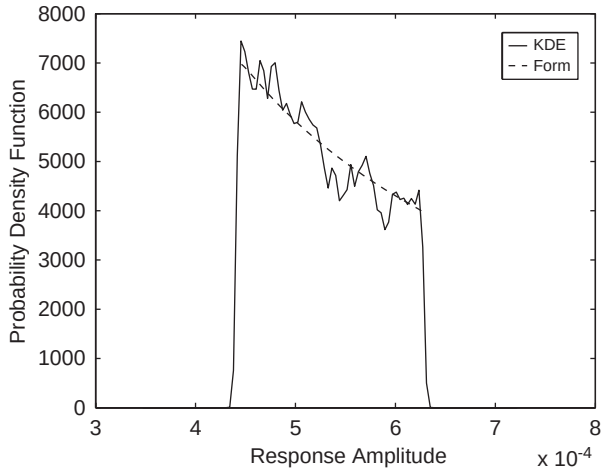

Fig. 16. Estimates of linear system response PDF. KDE (solid), Form (dashed).

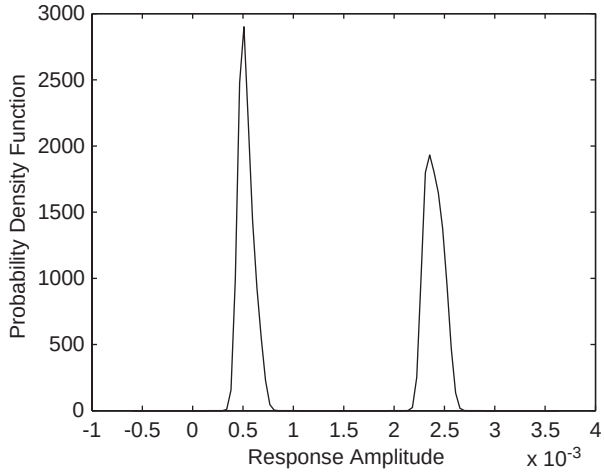

Fig. 17. Kernel density estimate of nonlinear system response PDF.

never happens and the calculation is abandoned when the step size is at machine precision. It should be emphasised that this is *not* a problem with the software implementation, but with the FORM method. One also observes that SORM would behave even more badly as a result of trying to estimate the Hessian.

7. Choice of uncertainty theory

The failure of the two methods discussed in the previous sections can be attributed to the fact that a probabilistic description of the uncertainty was attempted. In both cases, the particular

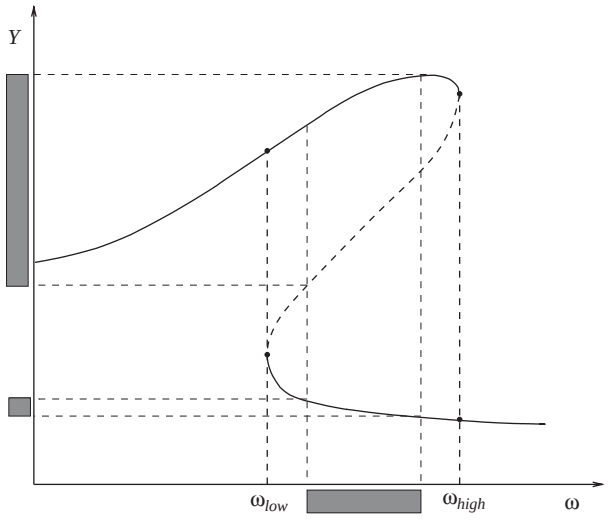

Fig. 18. Interval analysis 'solution' of nonlinear response problem.

pathology of the nonlinear system violated the basic requirements of the theory. In fact, there are many uncertainty frameworks available, commonly used examples are: evidence or Dempster–-Shafer theory [12,13], possibility theory [14], fuzzy logic [15], interval analysis [16] (and variants like affine arithmetic [17]) and convex models and information-gap theory [18,19]. (It is important to stress that this section is not intended as a critique of probabilistic analysis in general. Many modern developments in modern probabilistic reliability theory have simple been ignored here. The intention is simply to raise that alternative uncertainty theories may also applied with success.)

In terms of the nonlinear system problem of this paper, one might speculate that one of these alternative uncertainty formulations might be more suitable. In fact this is the case and the trick is to relax the requirements of the theory and move to *interval analysis* [16]. Asking for a probabilistic decription of the response amplitude was simply asking for too much. If one does not require a density, i.e. one simply asks for the support of the response, interval analysis allows the use of the harmonic balance FRF shown in Fig. 1 to give a qualitative solution of the problem as in Fig. 18. The important feature of the response—its bimodality is immediately obvious. Note that Fig. 18 is just a schematic and does not depict any of the detailed calculations carried out earlier.

8. Conclusions

There are essentially two threads to this paper. The first is to raise the issue that nonlinearity is likely to present problems for uncertainty analysis. This is not a particularly startling statement in itself, but the paper illustrates the point by presenting a simple nonlinear system which presents unsolvable problems; at least unsolvable in the context of the basic methods applied. (The reader should note that there is a huge literature in probabilistic reliability theory describing a broad

range of techniques which are simply not discussed here.) Great care should be taken in extrapolating from the simple system here to the highly complex computer simulations currently being undertaken and this is because the behaviour of nonlinear structural systems with very high numbers of degrees of freedom is simply not understood.

The last section shows very briefly that alternative uncertainty theories can be used profitably in situations where probabilistic methods fail and allows a return to the thesis discussed in the introduction to this article, namely that, in terms of uncertainty analysis, structural dynamics has arguably three main concerns: quantification of uncertainty in the context of the main theories, fusion of descriptions by different theories and propagation of uncertainty through systems and processes. The solution of these problems with any degree of comprehensiveness is a huge task and will occupy many researchers for many years.

Acknowledgements

KW would like to thank Drs. Francois Hemez and Scott Doebling of Los Alamos National Laboratory, New Mexico, USA, for many useful discussions and for inviting an earlier verison of this paper for presentation in a special session of the International Modal Analysis Conference. KW and MIF would also like to thank the EPSRC for providing the funding which allowed them to collaborate on this paper.

References

[1] N.C. Rasmussen, the U.S. Atomic Energy Commission and the U.S. Nuclear Regulatory Commission NUREG-75/014, WASH-1400, reactor safety study: an assessment accident risks in U.S. commercial nuclear power plants, 1975.

[2] M. Anderson, *Presentation at Workshop on Model Validation and Uncertainty Quantification at the 19th International Modal Analysis Conference*, Orlando, Florida, Uncertainty quantification at Los Alamos National Laboratories, 2002.

[3] K. Worden, On jump frequencies in the response of the Duffing oscillator, *Journal of Sound and Vibration* 198 (1996) 522–525.

[4] S.W. Doebling, F.M. Hemez, Model Validation and Uncertainty Quantification, Short Course Notes, Los Alamos Dynamics, 2001.

[5] J.M.T. Thompson, H.B. Stewart, *Nonlinear Dynamics and Chaos*, second ed., Wiley, New York, 2001.

[6] Ch.K. Chui, *An Introduction to Wavelets*, Academic Press, Inc., San Diego, 1992.

[7] Y. Meyer, *Wavelets. Algorithms and Applications*, SIAM, Philadelphia, 1993.

[8] G.W. Wornell, *Signal Processing with Fractals: A Wavelet Based Approach*, Prentice-Hall Signal Processing Series, Prentice-Hall, Englewood Cliffs, NJ, 1996.

[9] R.E. Melchers, *Structural Reliability Analysis and Prediction*, second ed., Wiley, New York, 1999.

[10] B.W. Silverman, *Density Estimation for Statistics and Data Analysis*, Chapman & Hall Monographs on Statistics and Applied, Probability, vol. 26, Chapman & Hall, London, 1986.

[11] FERUM Code and Manual available from: http://www.ce.berkeley.edu/~haukaas.

[12] A.P. Dempster, Upper and lower probabilities induced by a multi-valued mapping, *Annals of Mathematical Statistics* 38 (1967) 325–339.

[13] G. Shafer, *A Mathematical Theory of Evidence*, Princeton University Press, Princeton NJ, 1976.

[14] D. Dubois, H. Prade, *Possibility Theory: An Approach to Computerised Processing of Uncertainty*, Plenum Press, New York, 1986.
[15] L.A. Zadeh, Fuzzy sets, *Information and Control* 8 (1965) 338–353.
[16] R.E. Moore, *Methods and Applications of Interval Analysis*, SIAM, Philadelphia, PA, 1979.
[17] J.L.D. Comba, J. Stolfi, *Proceedings of SIBGRAPH '93*, Affine arithmetic and its applications to computer graphics, 1993, pp. 9–18.
[18] Y. Ben-Haim, I. Elishakoff, *Convex Models of Uncertainty in Applied Mechanics*, Elsevier, Amsterdam, 1990.
[19] Y. Ben-Haim, Set-models of information-gap uncertainty: axioms and an inference scheme, *Journal of the Franklyn Institute* 336 (1999) 1093–1117.